# Processing Full-Waveform Lidar Data: Modelling Raw Signals

Adrien Chauve, Clément Mallet, Frédéric Bretar, Sylvie Durrieu, Marc Pierrot-Deseilligny, William Puech

# PROCESSING FULL-WAVEFORM LIDAR DATA: MODELLING RAW SIGNALS

**Adrien Chauve[1,2,3], Clément Mallet[1], Frédéric Bretar[1], Sylvie Durrieu[2], Marc Pierrot Deseilligny[1] and William Puech[3]**

[1] Laboratoire MATIS - Institut Géographique National
2-4 av. Pasteur, 94165 Saint-Mandé, France - firstname.lastname@ign.fr
[2] UMR TETIS Cemagref/Cirad/ENGREF-AgroParisTech, Maison de la Télédétection
500, rue J.F. Breton 34093 Montpellier Cedex 5, France - firstname.lastname@teledetection.fr
[3] Laboratoire LIRMM, UMR CNRS 5506, Université Montpellier II
161, rue Ada, 34392 Montpellier Cedex 05, France - firstname.lastname@lirmm.fr

**KEY WORDS:** lidar, waveform analysis, signal processing, modelling, generalized Gaussian

**ABSTRACT:**

Unlike airborne multi-echo laser scanner systems, full-waveform systems are able to digitize and record the entire backscattered signal of each laser pulse. It has been demonstrated that decomposing the return waveforms into a mixture of Gaussian components was suitable. In this paper, we focus on the improvement of peak detection and of raw signal modelling. Refined peak detection greatly increased the number of detected targets as well as their positional accuracy. Models more complex than the Gaussian model, such as the Lognormal or generalized Gaussian functions, were introduced and their contribution to waveform processing was studied. In this way, fitting of asymmetric, peaked or flattened echoes located both in urban and forested areas could be improved. Moreover, introduction of new echo parameters allowed the extraction of additional information on the target shape. This should make easier the decorrelation of geometric and radiometric influences on the signal and, as a consequence, the improvement of point cloud classification algorithms.

## 1 INTRODUCTION

Airborne laser scanning is an active remote sensing technique providing range measurements between the laser scanner and the Earth topography. Well-known direct georeferencing processes turn such distance measurements into 3D point clouds with high accuracy and relevancy. Even for small footprints, there may be several objects of different range within the travel path of the laser pulse that generate individual backscattered echoes. Consequently, conventional lidar systems measure the first echo of the incoming signal ("first pulse") and the last echo ("last pulse"). Some are able to measure up to six pulses and more advanced systems also provide signal intensity.

During the last decade, a new generation of airborne laser scanners that are able to digitize and record the entire backscattered signal of each emitted pulse has appeared. They are called **full-waveform (FW)** lidar systems.
Historically, the first FW lidar systems were designed in the 1980s for bathymetric purposes (Guenther and Mesick, 1988). The first operational topographic system, developed by the NASA, appeared in 1999. The LVIS sensor (Laser Vegetation Imaging Sensor) was an improved version of a former satellite system, SLICER, developed in 1994 (Blair et al., 1999). SLICER was designed to describe the vertical structure of the canopy over extensive areas (Harding et al., 2001). LVIS data processing demonstrated the potential of recording return waveforms to characterize woodland areas and to measure the Earth topography, even ground beneath the canopy. First algorithms for classifying ground points by analysing the return waveform were developed and then resumed for the following system, GLAS, carried by the ICESAT satellite (2003-2006) (Zwally et al., 2002).
The first airborne commercial full-waveform lidar system has been operational since 2004 (LiteMapper-5600 lidar system based on the Riegl LMS-Q560 laser scanner) (Hug et al., 2004) and several features are now available for cartographic purposes.

Full waveform data hold large potentialities since it may overcome many drawbacks of classical multi-echo lidar data. More control is given to an end user in the interpretation process of the physical measurement. FW lidar data yield more than a basic geometric representation of the Earth topography. Instead of 3D point clouds, more detailed and additional information are provided about the structure of the illuminated surfaces with off-line processes. Thus, in addition to single range measurements, further physical properties of the objects included in the diffraction cone may be found with a backscattered waveform analysis. For example, in vegetated areas, more 3D points may be extracted, low vegetation can be separated from ground and both canopy and ground heights can be measured with higher accuracy (Dubayah and Blair, 2000).

Many studies have already been carried out to perform full waveform lidar data processing and analysis. Return waveform (1D signal) processing to extract more information than a single range measurement is the first main step. Non-linear least-squares (NLS) methods (Hofton et al., 2000, Reitberger et al., 2006) or maximum likelihood estimation using the Expectation Maximization (EM) algorithm (Persson et al., 2005) are typically used to fit the signal to a mixture of Gaussian functions to detect and parametrize the peaks. It was found in general that small-footprint lidar waveforms can be well modelled with a sum of Gaussian pulses (Wagner et al., 2006).
Geometric and radiometric influence of the hit targets have not been yet decorrelated. Therefore, point cloud segmentation algorithms using peak intensity and width still lead to a certain rate of misclassification without a good theoretical understanding of the waveform response for different targets (Ducic et al., 2006).

The aim of this study is to investigate further lidar return waveform processing. First, a raw signal modelling is proposed with Gaussian, Lognormal and generalized Gaussian functions. Indeed, waveforms can be very similar to an ideal Gaussian function (Wagner et al., 2006) whereas other laser impulse responses are slightly asymmetric (Hofton et al., 2000, Jutzi and Stilla, 2006). Consequently, approximating the waveforms using a sum of Gaussians may not be an accurate representation depending on the application and the target.

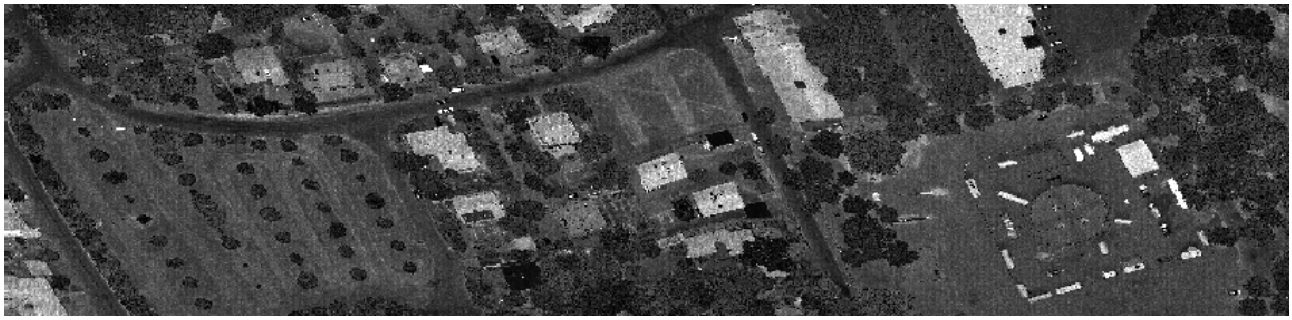

Figure 1: Amplitude image of the first echoes detected by the embedded real-time system, displayed in the sensor geometry.

A NLS algorithm is then performed with robust initial parameter estimates to improve usual approaches.
Finally, the contribution of proposed functions is discussed as well as the potentialities of new echo parameters for both urban and vegetation area mapping.

## 2 FULL-WAVEFORM LIDAR DATA

The data acquisition was performed in September 2006 with the RIEGL LMS-Q560 system over the city of Biberach (Bade Wutermberg, Germany). The main technical characteristics of this sensor are presented in (Wagner et al., 2006). The lidar system operated at a pulse rate of 100 kHz. The flight altitude was about 500 m and the footprint size was 0.25 m. RIEGL full-waveform system allows to determine the vertical distribution of targets within the diffraction cone with a temporal resolution of around 1 ns. The target resolution of the system is close to 0.6 m and the spatial resolution (*i.e.* the distance between two samples) is 0.3 m. The surveyed area includes both residential, industrial and dense vegetated areas (figure 1). The point density is about 2.5 pts/m$^2$.

Each return waveform is composed of one or two sequences of 60 samples that is to say an altimetric profile of 18 m (or 36 m). For each emitted pulse, the emitted signal (60 samples) and the echoes found by the embedded real-time detection algorithm are given as well as their amplitude and width (figure 2).

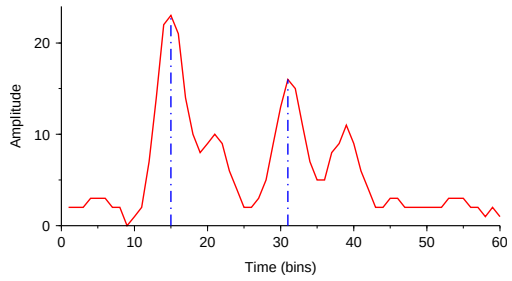


Figure 2: Example of a measured waveform for RIEGL LMS-Q560 system. Dashed lines indicate the position of the echoes detected by the system. The background noise is relatively low within the observed waveforms.

## 3 WAVEFORM PROCESSING

Waveform processing consists in decomposing the waveform into a sum of components or echoes, so as to characterise the different targets along the path of the laser beam. It is a parametric approach to estimate a mathematical model. The aim of waveform processing is therefore to extract as many peaks from the signal as possible, but also information for each echo. It consists in two main steps : first, the number of components and initial values are estimated. Then the parameters are optimized. The optimization process is well-known and it has been demonstrated that either the Expectation-Maximization algorithm (Maximum Likelihood estimates) (Persson et al., 2005) or the Levenberg-Marquardt algorithm (non-linear least-squares method) (Hofton et al., 2000, Wagner et al., 2006) give good results. Nevertheless, optimization relies strongly on initial parameters. They therefore must be estimated very carefully to avoid erroneous results. In this study, an improvement of usual peak detection has been first performed. Then a new waveform modelling has been proposed with different functions to improve signal fitting.

### 3.1 Methodology

A full waveform extracted from the RIEGL LMS-Q560 system is composed of one or two sequences of 60 points uniformly-spaced $\{(x_i, y_i)\}_{i=1,..,N}$ sampled at 1 GHz. We aim at decomposing each sequence into a sum of components representing the targets located within the travel path of the laser beam as

$$y = f(x) = \sum_{j=1}^{n} f_j(x) \quad (1)$$

where $n$ is the number of components, $f_j$ a given function that may be a Gaussian, Lognormal or a generalized Gaussian (see section 3.3).

For each sequence, the background noise is first thresholded. Then, a basic detection method is used to estimate the number and the position of the components. Other function parameters are fixed with constant values. A first fit is computed, using a non-linear least-squares method. A fine detection using the fitting result is then performed to find missing peaks (cases of complex overlapping echoes, see figure 3). If new peaks are detected, a second fit is processed with the same method.

### 3.2 Peak detection and initial parameters estimation

The basic detection method is based on the zero crossings of the first derivative on the thresholded version of the waveform. The detection algorithm takes into account a minimal number of samples separating two detected peaks (spatial resolution of the system). A non-linear least-squares method with the Levenberg-Marquardt algorithm implemented in the GSL (GNU Scientific Library) is then used to compute the fit. The quality of the results

is evaluated by

$$\xi = \frac{1}{N-p} \sum_{k=1}^{N} (y_k - f(x_k))^2 \qquad (2)$$

where the numerator is the sum of the residual differences between the observed waveform and the fitting function, $N$ is the number of samples and $p$ is the number of parameters of the fitting function.

In case of complex overlapping echoes, zero crossings of the first derivative are not sufficient to detect all real peaks. Indeed, a finer peak detection is needed when two overlapping echoes are so close that a single maximum is found, but three inflexion points (instead of two for a standard echo) exist. One solution is to perform a second pulse detection on the thresholded difference between the observed waveform and the previous fit. If a peak is detected, a new fit is run with the new component. The resulting $\xi$ value is compared to the previous one and this step is repeated until the $\xi$ factor stops decreasing.

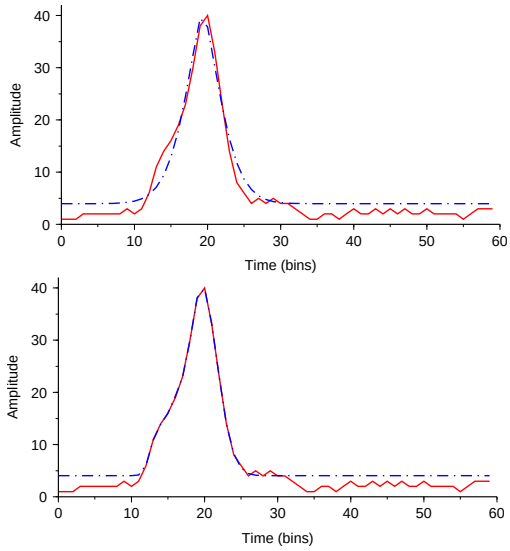


Figure 3: Example of complex waveform. The RIEGL system data is in red colour (continuous line) and the fitted result in blue (dashed line). Data is first thresholded to the value of 4 before pulse detection. **Top:** Fit with only a coarse pulse detection. **Bottom:** Fit with a fine detection. Two echoes are now found.

### 3.3 Modelling functions

Each laser output pulse shape is assumed to be Gaussian, with a specific and calibrated width. The collected pulse is therefore a convolution between this Gaussian distribution and a "surface" function, depending on the hit objects. It has been shown that if the vertical height distribution of the elements within the diffraction cone follows a Gaussian law, the reflected waveform can be approximated by a sum of Gaussians (Zwally et al., 2002). Wagner (Wagner et al., 2006) has shown that more than 98% of the observed waveforms with the RIEGL system could be fitted with a sum of Gaussian functions.

Nevertheless, this assumption is not always satisfactory. Depending on the lidar system, the transmitted signal is not always Gaussian but can be slightly distorted (asymmetric, flattened or peaked). For the LMS-Q560 waveforms, a steeper ascending part as well as a longer but weaker descending one than the Gaussian model can be noticed. Moreover, the Gaussian height distribution of the targets has only be statistically shown for large-footprint lidar systems (Carabajal et al., 1999). For small-footprint systems, there is no assuming that the height distribution is Gaussian, even over vegetated areas. Therefore modelling full-waveform lidar data with a sum of Gaussian functions can be inaccurate. It is of interest to extend waveform processing capabilities by using more complex parametric models. It enables to both improve signal fitting and extract more information from the raw signal. Standard extensions of Gaussians are Lognormal and generalized Gaussian functions. The detected peaks can be asymmetric and modelled with a Lognormal function (see figure 4a). Besides, some symmetric waveforms are observed to be distorted over forested areas and over some building roofs. Using the generalized Gaussian model (see figure 4b) can improve signal fitting for complex waveform shapes.

Gaussian (G), Lognormal (L) and generalized Gaussian (GG) models have the following analytical expressions (see figure 4 for plots) :

$$f_{\mathrm{G},j}(x) = a_j \exp\left(-\frac{(x-\mu_j)^2}{2\sigma_j^2}\right) \qquad (3)$$

$$f_{\mathrm{L},j}(x) = a_j \exp\left(-\frac{(\ln(x-s_j)-\mu_j)^2}{2\sigma_j^2}\right) \qquad (4)$$

$$f_{\mathrm{GG},j}(x) = a_j \exp\left(-\frac{|x-\mu_j|^{\alpha_j^2}}{2\sigma_j^2}\right) \qquad (5)$$

The observation of data on the whole survey area shows that most of the asymmetric peaks are in fact so close overlapping echoes that the third inflexion point is hardly visible. As a consequence, with the coarse pulse detection, fitting the waveform with a mixture of Lognormal results in a better quality of fit (*i.e.* a lower value of $\xi$) than fitting with a sum of Gaussians. However, improving the peak detection as presented before leads to the detection of two echoes. Gaussian fitting is then better.

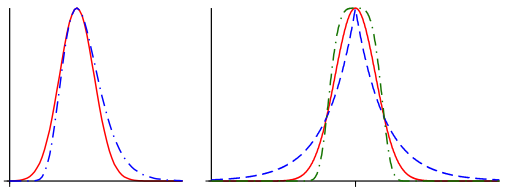

Figure 4: **Left:** Comparison between Gaussian (continuous line) and Lognormal (dotted line) functions. **Right:** The generalized Gaussian function: $\alpha$=1 = Laplace function (dashed line), $\alpha$=$\sqrt{2}$ = Gaussian function (continuous line) and $\alpha$=2 (dotted line).

The generalized Gaussian model enables to simulate both Gaussian shapes when $\alpha = \sqrt{2}$, peaked shapes when $1 \leq \alpha < \sqrt{2}$ ($\alpha = 1$ gives the Laplace function) and flattened shapes when $\alpha > \sqrt{2}$ (see figure 4b). Therefore it should improve the quality of the fit in most of the cases. But with a simple NLS algorithm, it will also increase the number of fits that do not converge, just like the Lognormal. It is due to the increasing number of degrees of freedom of the function and also to the more complex expression of the gradient (Aiazzi et al., 1999).
The generalized Gaussian is also used to model SAR amplitude (Moser et al., 2006), image texture or even outliers in image matching (Hasler et al., 2003). The $\alpha$ parameter is yet very interesting for waveform analysis because it provides another piece of information about the shapes of the echoes, in addition to their width, and it could be useful for classification purposes (see section 4.3).

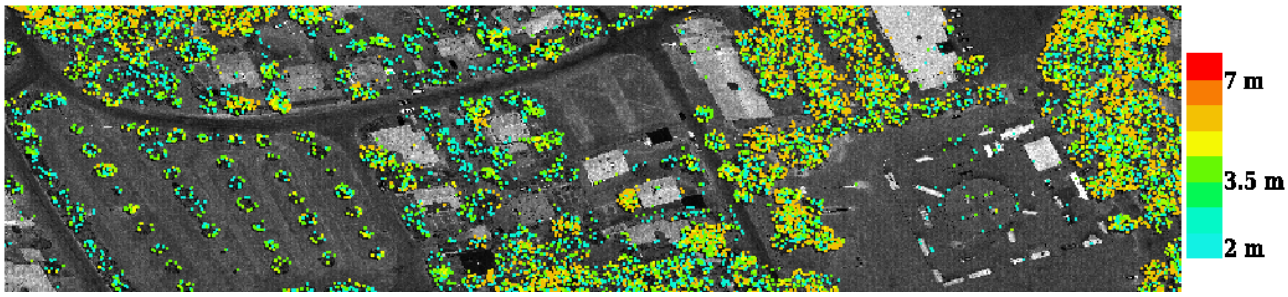


Figure 5: Difference of last pulse altitude between post-processing algorithm and real-time process. Only height differences greater than 2 m has been displayed.

## 4 RESULTS AND DISCUSSION

### 4.1 Point extraction

Lidar waveform post-processing allows to densify the final point cloud up to 50 % on forested areas (see table 1). The Gaussian fit was successful for about 99.3% of waveform profiles. A waveform was considered to be well fitted if the quality factor $\xi < 0.5$. It has been observed that $\xi < 0.1$ on urban areas with a single pulse of Gaussian shape and that $\xi \leq 0.5$ even for complex targets consistently fitted.

Analysing the differences between fitted waveforms and the delivered point cloud, one can notice that weak and overlapping echoes are now detected. As expected, the additional points are located near the tree canopy and in low ground vegetation areas. Only few points are additionally detected on the ground beneath the canopy, due to the survey low point density and the small laser footprint. Finally, more echoes are also detected on artificial objects in urban areas, because of multiple pulse reflections at building edges.

The fine peak detection performed after the first two steps (coarse detection and signal fitting) allows to detect up to 10 % more points than a unique coarse echo detection. Low intensity echoes close to strong ones are henceforth extracted (figure 3). The quality of the fit is therefore improved: figure 6 shows a significant decreasing of $\xi$ median value. The fine peak detection enhances the stability of NLS method whatever the fitting function. Indeed, when providing relevant estimates of echo positions as input data, the fitting procedure finds a solution for almost all return profiles (99.99 % for the Gaussian, 99.8 % for the the generalized Gaussian and 99.05 % for the Lognormal function).

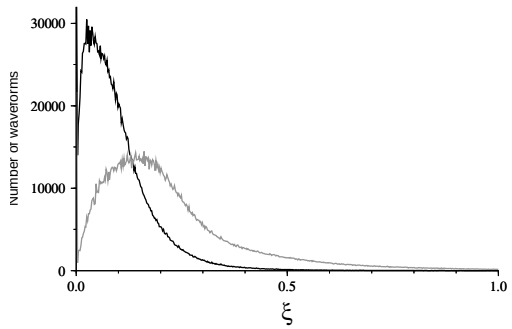


Figure 6: Histogram of $\xi$ values for the Gaussian model : coarse detection (black) and fine detection (grey).

As expected, full-waveform lidar data enables to penetrate deeper in forested areas. Nevertheless, there is still no assuming the last detected pulse is the ground. Figure 5 shows the difference of last pulse altitude between post-processing algorithm and real-time method. It illustrates that extracted points are significantly closer to the ground over vegetated areas (until 10 m). Moreover, the first pulse detection is also bettered over vegetated areas. Statistical results are summarized in table 1 where the mean difference $\Delta$Height between post-processing detected pulse height and real-time one is always positive for the last pulse (*e.g.* $+1.58$ m for dense vegetation) and always negative for the first pulse (*e.g.* $-0.42$ m).

| Area | Whole Area | Dense Vegetation | Vegetation | Residential | Downtown |
|---|---|---|---|---|---|
| **Nb profiles** | 2027547 | 70074 | 23368 | 93690 | 66264 |
| **Non fitted (%)** | 0.01 | 0.004 | 0.008 | 0.01 | 0.02 |
| **Nb points extracted** | 2903976 | 147218 | 46246 | 120813 | 85520 |
| **Additional points (%)** | 24 | **55** | **51** | 9 | 10 |
| **$\Delta$Height first (m)** | -0.13 | -0.42 | -0.34 | -0.04 | -0.04 |
| **$\Delta$Height last (m)** | 0.36 | 1.58 | 1.36 | 0.07 | 0.05 |

Table 1: Statistics on point extraction on different test areas. The figures of non-fitted profiles and difference of height measurement are given for the Gaussian model.

### 4.2 Comparison between modelling functions

As mentioned in other publications (Reitberger et al., 2006, Wagner et al., 2006), the Gaussian decomposition of lidar waveforms is a good approximation of the signal ($\xi < 0.5$ for 99.3% of the processed waveforms).
$\xi > 0.5$ means that the Gaussian model is not appropriate for modelling complex waveform. Such values are particularly observed on forested areas. Even for small $\xi$ values, the Gaussian decomposition can be inaccurate. Indeed, for high and narrow echoes as well as for weak and large ones, Gaussian fitting could be improved. Such cases are difficult to quantify.

Modelling raw signals with the **Lognormal function** does not improve the waveform fitting for the whole survey area but locally. $\xi$ values are globally higher than for the Gaussian model. Besides, inconsistencies are found for more than 5 % (*i.e.* $\xi > 5$) and the NLS algorithm diverges more often than for other functions (1 % compared to 0.01 % for the Gaussian model).
Nevertheless, in very few cases, $\xi$ values are lower for the Lognormal decomposition than for a sum of Gaussians. It shows that some backscattered echoes are asymmetric. Such cases are observed on streets and some building roofs. Further experiments have to be carried out to draw more conclusions.
It seems that a high value of $\xi$ only means that the lidar waveform is not well modelled with Lognormal functions. But it does not mean that all the waveform echoes are inconsistently modelled. Thus modelling waveforms with a sum of different functions could be appropriate.

The **generalized Gaussian** function allows to model flattened, narrow and high pulses. $\xi$ values are lower for such model than for the Gaussian function. Figure 7 shows the $\xi$ histograms of Gaussian and generalized Gaussian models. The latter improves the global fitting quality. Still a higher number of inconsistent fitting results is noticed (about 0.4%). Theoretically the generalized Gaussian should always fit at least as well as the Gaussian function. But in practice, this is due to a minimization problem in the NLS method.
In the streets (asphalt or pavement), the fitting procedure works as well as for the Lognormal function. Indeed, the observed pulses have a high intensity and a low width ($\alpha \rightarrow 5$), what can be well modelled with the Lognormal function. But for asymmetric echoes, the generalized Gaussian model is not suitable.

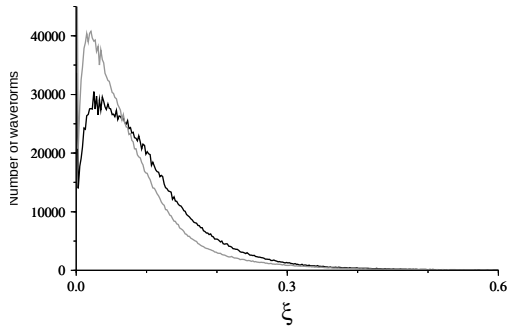


Figure 7: Histogram of $\xi$ values for Gaussian fit (black) and generalized Gaussian fit (grey) using fine detection.

### 4.3 Contribution of the generalized Gaussian function

As expected, the generalized Gaussian model improves signal fitting. Furthermore, a new parameter $\alpha$ is estimated giving information about the sharpness of the detected echo. The parametric description of the targets given by the signal processing step contains significant information on the roughness, slope and reflectivity of the target surface. The main issue is that geometric and radiometric influences are correlated in one single shape. It seems difficult to decorrelate them with only return intensity and pulse width estimation.
A close observation of the data gives some hints on an empirical classification based on $\alpha$:

- $\alpha > 1.9$ (rare) concerns pulses belonging to building edges and both to the top of the canopy and below the canopy. Simulations have to be performed to investigate whether echoes in forested areas concern low ground vegetation or bare ground;
- $1.6 < \alpha < 1.9$ is typical of vegetated areas (first echoes more than the other ones) but also of artificial planar areas (asphalt streets for example);
- $1.3 < \alpha < 1.6$ (associated to Gaussian shape) is found on natural ground (beaten-earth floor, grass) and building roofs;
- $\alpha$ <1.3 (very rare) concerns tree canopy and building boundaries.

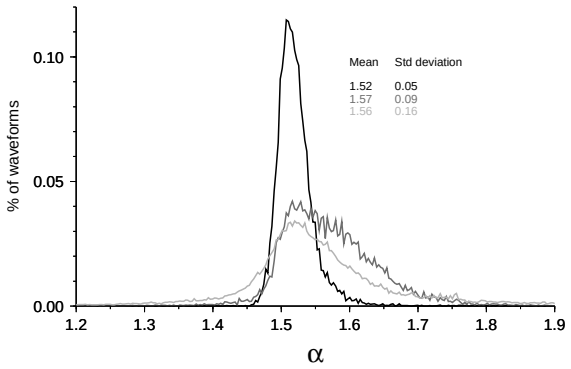


Figure 8: Histogram of $\alpha$ values over three homogeneous test areas (more than 15000 waveforms each) : building roofs (black), asphalt streets (dark grey) and dense vegetation (grey).

Figure 8 shows the distribution of $\alpha$ values over three test areas. The three mean values are all close to 1.55, meaning that the general shape of the backscattered echoes is close to a slightly flattened Gaussian. Extreme values ($< 1.3$ and $> 1.9$) are found on forested areas where, for small-footprint lidar systems, there is no assuming the value of the shape parameter. For urban areas, it can help to segment building and artificial ground areas. Further work have to be done to perform such classification algorithm, maybe with the help of both intensity and width pulse values.

The potentialities of the scale parameter $\alpha$ of the generalized Gaussian model can be shown on terrain areas. On flat areas, $\alpha$ seems less sensitive to radiometric changes than the two other ones. For example, intensity and width values are affected by the presence of zebra-crossings on the streets, of tracks on car parks, of moisture on natural surfaces, whereas $\alpha$ parameter is estimated almost constant. It could therefore be useful to classify geometrically similar areas as shown in figure 9. Although $\alpha$ values images are very noisy, $\alpha$ could be a discriminative parameter if associated to other variables in a supervised classification framework.

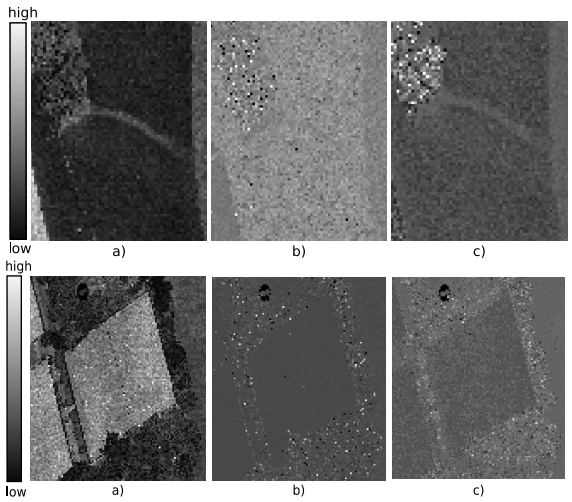


Figure 9: Comparison between the amplitude (**a**), $\alpha$ (**b**) and width parameters (**c**) on artificial (tracks on car park, **top**) and natural (moisture on tennis courts, **bottom**) ground areas.

## 5 CONCLUSIONS AND FUTURE WORK

The problem of modelling full-waveform lidar data has been investigated in this paper. It is known that the decomposition of an observed lidar waveform into its components not only improves the ranging accuracy of the measurement but also enables the determination of the heights of various reflecting surfaces within the laser diffraction cone. The traditional Gaussian fitting gives in general good results for all kind of areas. Providing the intensity and the width for each echo is however not sufficient for classification purposes.

We introduced the mixture of Lognormal functions to fit asymmetric echoes, especially on streets and roofs. Nevertheless, such model is not suitable for eclectic landscapes. The main limitation is that return bumps are not always of the same nature: it can be a mixture of Lognormal, Gaussian and other functions. We finally introduced the generalized Gaussian model to fit distorted peaks and still enables to fit Gaussian shapes. The modelling methodology is thus improved compared to the Gaussian adjustment. A practical limitation has however been observed since the fitting procedure gives inconsistent results for several waveforms due to optimization problems in the NLS method. But the contribution of this function is all the more significant since a new parameter is estimated for each peak, providing new information about its shape. A first visualization shows its potentialities for classifying extracted point cloud especially in urban areas. Waveform simulations have to be carried out to understand its global contribution.

Improving peak detection was shown in this paper to be very successful to extract additional targets in the return waveforms. However, for classification purposes, it could be more interesting to fit a wide flattened echo with only one generalized Gaussian instead of two basic Gaussians: parameter $\alpha$ would provide information to classify the group of two overlapping echoes that otherwise would not be available. Depending on the application, two approaches are conceivable. On the first hand a coarse pulse detection with a suitable model can be used for classification. On the other hand, an improved point detection with just a Gaussian model can be performed to describe accurately 3D vegetation structure.

Both Lognormal and generalized Gaussian functions contribute to improve lidar waveform modelling but not in the same way. Consequently, the three functions have to be gathered to take benefit from their specific advantages. Besides, other suitable functions have to be tested in order to best describe the return waveform. As the Gaussian fitting is already almost successful all the time, new modelling functions with different parameters have to be found. They could provide new information about the peaks and therefore contribute to lidar point cloud segmentation.
A combination of several suitable functions have therefore to be performed to assess this solution. A Reversible Jump Monte Carlo Markov Chain (RJMCMC) method could, for example, be implemented thanks to its high flexibility. Jumps between models of different dimensions (the number of parameters) are possible and consequently each raw signal can be segmented by different functions.

## ACKNOWLEDGEMENTS

The authors would like to thank Toposys for providing test data, as well as Boris Jutzi for fruitful discussions.

## REFERENCES

Aiazzi, B., Alparone, L. and Baronti, S., 1999. Estimation based on entropy matching for generalized Gaussian PDF modeling. IEEE Signal Processing Letters 6(6), pp. 138–140.

Blair, J., Rabine, D. and Hofton, M., 1999. The Laser Vegetation Imaging Sensor: a medium-altitude digitisation-only, airborne laser altimeter for mapping vegetation and topography. ISPRS Journal of Photogrammetry and Remote Sensing 54, pp. 115–122.

Carabajal, C., Harding, D., Luthcke, S., Fong, W., Rowton, S. and Frawley, J., 1999. Processing of Shuttle Laser Altimeter range and return pulse data in support of SLA-02. In: ISPRS Workshop 'Mapping Surface structure and topography by airborne and spaceborne lasers', Vol. XXXII-3/W14, La Jolla, United States.

Dubayah, R. and Blair, J., 2000. Lidar Remote Sensing for Forestry Applications. Journal of Forestry 98(6), pp. 44–46.

Ducic, V., Hollaus, M., Ullrich, A., Wagner, W. and Melzer, T., 2006. 3D Vegetation mapping and classification using full-waveform laser scanning. In: Workshop on 3D Remote Sensing in Forestry, Vienna, Austria.

Guenther, G. and Mesick, H., 1988. Analysis of airborne lidar bathymetric waveforms. In: Proc. of SPIE Ocean Optics IX, Orlando, United States, pp. 232–241.

Harding, D., Lefsky, M. and Parker, G., 2001. Laser altimeter canopy heigh profiles. Methods and validation for closed-canopy, broadleaf forests. Remote Sensing of Environment 76(9), pp. 283–297.

Hasler, D., Sbaiz, L., Susstrunk, S. and Vetterli, M., 2003. Outlier modelling in image matching. IEEE Trans. on Pattern Analysis and Machine Intelligence 25(3), pp. 301–315.

Hofton, M., Minster, J. and Blair, J., 2000. Decomposition of Laser Altimeter Waveforms. IEEE Transactions on Geoscience and Remote Sensing 38(4), pp. 1989–1996.

Hug, C., Ullrich, A. and Grimm, A., 2004. Litemapper-5600 - A Waveform-Digitizing LIDAR Terrain and Vegetation Mapping System. In: ISPRS Laser-Scanners for Forest and Landscape Assessment, Vol. 36, Frieburg, Germany.

Jutzi, B. and Stilla, U., 2006. Range determination with waveform recording laser systems using a Wiener Filter. ISPRS Journal of Photogrammetry and Remote Sensing 61, pp. 95–107.

Moser, G., Zerubia, J. and Serpico., S., 2006. Sar amplitude probability density function estimation based on a generalized gaussian model. IEEE Trans. on Image Processing 15(6), pp. 1429–1442.

Persson, A., Söderman, U., Töpel, J. and Alhberg, S., 2005. Visualization and Analysis of Full-Waveform Airborne Laser Scanner Data. In: ISPRS workshop 'Laserscanning 2005', Enschede, The Netherlands, pp. 103–108.

Reitberger, J., Krzystek, P. and Stilla, U., 2006. Analysis of full-waveform lidar data for tree species classification. In: ISPRS Photogrammetric Computer Vision (PCV), Bonn, Germany, pp. 228–233.

Wagner, W., Ullrich, A., Ducic, V., Melzer, T. and Studnicka, N., 2006. Gaussian decomposition and calibration of a novel small-footprint full-waveform digitising airborne laser scanner. ISPRS Journal of Photogrammetry and Remote Sensing 66, pp. 100–112.

Zwally, H., Schutz, B., Abdalati, W., Abshire, J., Bentley, C., Brenner, A., Bufton, J., Dezio, J., Hancock, D., Harding, D., Herring, T., Minster, B., Quinn, K., Palm, S., Spinhirne, J. and Thomas, R., 2002. ICESat's laser measurements of polar ice, atmosphere, ocean, and land. Journal of Geodynamics 34(3), pp. 405–445.